



# The modern and Last Glacial Maximum hydrological cycles of the Eastern Mediterranean and the Levant from a water isotope perspective



Y. Goldsmith<sup>a,\*</sup>, P.J. Polissar<sup>a</sup>, A. Ayalon<sup>b</sup>, M. Bar-Matthews<sup>b</sup>, P.B. deMenocal<sup>a</sup>, W.S. Broecker<sup>a</sup>

<sup>a</sup> Lamont–Doherty Earth Observatory of Columbia University, Palisades, NY, USA

<sup>b</sup> Geological Survey of Israel, 30 Malchei Israel Street, Jerusalem 95501, Israel

## ARTICLE INFO

### Article history:

Received 23 December 2015  
Received in revised form 6 October 2016  
Accepted 8 October 2016  
Available online 2 November 2016  
Editor: D. Vance

### Keywords:

stable isotopes  
speleothem  
Rayleigh distillation  
Last Glacial Maximum  
Israel  
Mediterranean

## ABSTRACT

The isotopic composition of precipitation ( $\delta p$ ) is one of the most widely used and informative terrestrial paleoclimate proxies.  $\delta p$  integrates a series of hydrological processes; therefore, any interpretation of paleohydrology using  $\delta p$  requires a thorough understanding and quantification of the full hydrological cycle. In this paper, we use modern data to analytically model the full isotopic hydrological cycle of the Eastern Mediterranean and the Southern Levant, including oceanic evaporation, distillation during transport and precipitation over land. This model allows us to determine the important factors controlling this system. The model results underscore the significance of the isotopic distillation process driven by the land–sea temperature gradient as a significant factor controlling the long-term average isotopic composition of precipitation across Israel. Based on the understanding of the processes that govern the modern system, we model the isotopic composition of precipitation from the Last Glacial Maximum (LGM) using published data for speleothem oxygen isotopes in calcite, oxygen and hydrogen isotopes in fluid inclusions and clumped isotope values from Soreq Cave and the isotopic composition of East Mediterranean planktonic foraminifera *G. ruber*. The data and model results indicate two plausible scenarios for the LGM that entail changes in the magnitude of distillation over Israel, in normalized humidity over the Mediterranean and possible shifts of the moisture trajectories over the Mediterranean. The results presented in the paper illustrate the importance of understanding the full local hydrological cycle when reconstructing and interpreting the isotopic composition of precipitation.

© 2016 Elsevier B.V. All rights reserved.

## 1. Introduction

The isotopic composition of precipitation is widely used to constrain modern hydrological process and past terrestrial climate. The isotopic signal is acquired through a sequential series of hydrological steps, which require quantification in order to produce reliable climatic interpretations based on the isotopic composition of precipitation. In prior work, the contributions of moisture sourcing (e.g. Pausata et al., 2011) and the isotopic composition of vapor (e.g. Good et al., 2015) to the isotopic composition of precipitation have been established. These realizations must thus be incorporated into paleoclimate interpretations of isotope records. In this paper, we present a methodology for analyzing and interpreting modern and paleo-rainfall isotopic data. We first investigate the

modern hydrological cycle and show that it is possible to derive from first principles the major factors controlling the system. We then use these principles to reinterpret isotopic records from the Last Glacial Maximum (LGM). The investigation is focused on the Eastern Mediterranean (EM) because of the wealth of modern and paleo-isotopic data that exists in this region, which enable identification of the major processes controlling the isotopic composition of precipitation.

The isotopic composition of modern precipitation in the EM and the Levant has gained much attention in the past four decades due to its uniquely high d-excess (defined as d-excess =  $\delta D - 8 \times \delta^{18}O$ , Dansgaard, 1964) in respect to the global isotope composition of precipitation (e.g. Gat and Dansgaard, 1972; Gat and Carmi, 1970, 1987; Gat et al., 2003; Ayalon et al., 2004; Angert et al., 2008) and due to its paleoclimate utility as a climate recorder in speleothems (e.g., Ayalon et al., 1998, 2013; Bar-Matthews et al., 1997, 1999, 2003; Frumkin et al., 1999; Orland et al., 2014) and lacustrine environments (Kolodny et al., 2005). Previous re-

\* Corresponding author.

E-mail address: yonig@ldeo.columbia.edu (Y. Goldsmith).

search conducted on the modern conditions in this region span short time periods (e.g. Gat and Carmi, 1970, 1987), are centered in specific sub-regions in Israel (e.g. Angert et al., 2008; Ayalon et al., 2013) or pertain to specific parts of the hydrological cycle (e.g. Gat et al., 2003). Although general models have been presented that describe how the unique composition of modern precipitation (e.g. Gat et al., 1996; and Gat and Carmi, 1970, 1987) and the paleohydrology of the EM (Gat and Dansgaard, 1972; Gat and Carmi, 1987; McGarry et al., 2004) were acquired, they are based on limited aspects of the hydrological cycle (i.e. vapor, precipitation etc.) and do not encompass the full hydrological cycle, which is composed of sea surface water, vapor, distillation, precipitation and evaporation. Here we analyze data from long-term monitoring of the isotopic composition of precipitation from 14 sites distributed across Israel and water and vapor data from the Mediterranean. Together, these data allow us to quantify the major processes that control the hydrological cycle of the Eastern Mediterranean and evaluate the processes that control the long-term average isotopic composition of precipitation in Israel.

### 1.1. Modern climatology of Israel

Rainfall in Israel occurs almost exclusively between Oct and Apr, with most of the rainfall falling between Dec and Feb. During the rainy season, cold-core, upper-level, low-pressure troughs propagate from west to east over southern Europe and the Mediterranean (Ziv et al., 2006). When dry air from Europe passes over the mountainous regions to the north of the Mediterranean it encounters the warm Mediterranean sea surface and forms the Cyprus Low, a cyclonic surface low-pressure system, which lifts the moistened marine air to produce clouds and precipitation (Fig. 1). These systems migrate eastward and deliver precipitation over Israel (Ziv et al., 2006) (Fig. 1).

The topography of Israel can be divided into three areas from West to East: the low coastal plain, a North-South mountainous region and the Dead Sea Valley (Fig. 1). Precipitation amount generally correlates with temperature and altitude, where greater precipitation falls at higher and colder elevations (Fig. 1). In addition, temperatures decrease and rainfall increases from South to North (Fig. 1). The southern part of Israel lies in the global desert belt and the northern part has a Mediterranean climate. The Dead Sea Valley is a local rain-shadow desert.

The climatic regime in Israel is, in many ways, ideal for isotopic study. As rainfall only occurs during winter there are no complications due to seasonality of precipitation. In addition, the cold temperatures during winter reduce evaporation from the base of the cloud and thus reduce the variability of the isotopic composition. The distance from the sea, elevation, temperature and latitude are all correlated, all driving the isotopic composition in the same direction. In addition, the short transport distance (<100 km) prevents significant moisture recycling.

### 1.2. Definitions and isotope notations

During phase changes in the hydrological cycle, fractionation occurs between the heavy and light isotopes of oxygen and hydrogen due to differences in their vibrational energy and thus their affinity for higher (e.g. gas) or lower (e.g. water) energy states. Therefore, the ratio of the heavy to light isotopes records the magnitude of these phase changes (Gat, 1996). The isotopic compositions of oxygen and hydrogen ( $\delta$ ) are reported in the delta notation:

$$\delta = \left( \frac{R_{(sample)}}{R_{(VSMOW)}} \right) - 1 \quad (1)$$

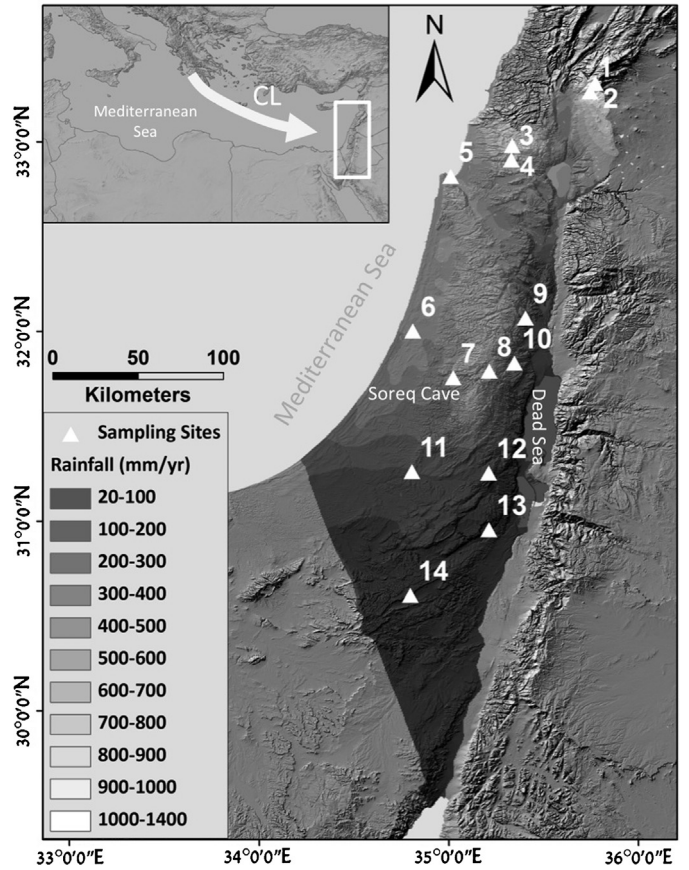


Fig. 1. An annual rainfall map of Israel (gray scale) superimposed on a shaded relief map, showing the rainfall sampling sites (white triangles) and locations mentioned in the text. The site numbers correspond to Table 1. The map at the top left shows the general location and direction of the modern Cyprus Low (CL) – the prominent path of moisture reaching Israel.

where  $R$  is the ratio of the heavy to light isotopes and VSMOW is the standard used. The calculations are performed using the abundance ratios, but for convenience the isotope data in the plots and tables are multiplied by  $10^3$  and presented in per-mil units (‰).

The equilibrium fractionation factor ( $\alpha_{l-v(T)}$ ), which is a function of the temperature, is defined as:

$$\alpha_{l-v(T)} = \frac{R_l}{R_v} \quad (2)$$

where  $R_l$  and  $R_v$  are the isotopic ratios in liquid and vapor, respectively. Majoube (1971) empirically calculated the fractionation factor as:

$$\ln \alpha_{l-v}^{18O} = \frac{1137}{T^2} - \frac{0.4156}{T} - 0.00207 \quad (3)$$

and

$$\ln \alpha_{l-v}^D = \frac{24844}{T^2} - \frac{76.248}{T} + 0.05261 \quad (4)$$

where  $T$  is the temperature in Kelvin.

During equilibrium processes, the relative magnitude of fractionation of oxygen and hydrogen  $(\alpha_D - 1)/(\alpha_{18O} - 1)$  cause hydrogen to fractionate  $\sim 8$  that of oxygen. Therefore, the isotopic composition of global precipitation falls on a slope of 8 when plotted on a  $\delta^{18O}$  vs.  $\delta D$  plot (Gat, 1996). The kinetic fractionation factor of oxygen is larger than that of hydrogen relative to equilibrium fractionation. Therefore, during kinetic fractionation, which predominantly occurs during evaporation at the moisture source (Merlivat and Jouzel, 1979), oxygen fractionates to a larger degree

**Table 1**  
Isotopic composition, temperature, elevation, distance from the sea and annual precipitation amount from 14 sites in Israel (for location of sites see Fig. 1). Temperatures in bold are calculated using equation (18) in Section 4.1.3.

Site number	Site	Number of years	Number of samples	Cumulative $\delta^{18}\text{O}$ (‰)	Standard error $\delta^{18}\text{O}$	Cumulative $\delta D$ (‰)	Standard error $\delta D$	Temp (K)	Elevation (masl)	Sea distance (km)	Rainfall (mm/yr)	$\alpha^{18}\text{O}$	$\alpha D$
1	Hermon	12	90	-7.3	0.2	-38.5	4.8	<b>277.4</b>	1660	64	1400	1.0113	1.106
2	Neve Ativ	10	103	-7.0	0.3	-34.8	1.2	<b>281.1</b>	1000	60	1200	1.0109	1.101
3	Peqilin	11	188	-6.2	0.2	-29.3	0.6	<b>283.2</b>	650	23	870	1.0107	1.098
4	Mikhmanim	12	607	-6.2	0.1	-29.2	0.8	<b>283.9</b>	531	24	590	1.0106	1.097
5	Haifa Port	2	95	-5.7	0.4	-25.6	1.6	287.9	30	0.5	539	1.0103	1.091
6	Bet Dagan	26	172	-5.1	0.1	-18.6	1.1	287.0	30	8	520	1.0103	1.093
7	Soreq	18	638	-5.5	0.1	-22.4	0.7	<b>285.4</b>	400	40	550	1.0105	1.095
8	Jerusalem	11	390	-6.3	0.2	-28.1	1.1	284.0	815	56	537	1.0106	1.097
9	Ma'ale Ephrayim	2	35	-4.6	1.5	-18.7	9.3	<b>286.3</b>	200	60	320	1.0104	1.094
10	Alon	9	273	-4.5	0.2	-19.3	2.2	<b>286.2</b>	250	66	330	1.0104	1.094
11	Beer Sheva	9	102	-4.5	0.2	-13.5	2.1	286.6	280	47	195	1.0104	1.093
12	Arad	9	40	-3.9	0.4	-14.4	2.8	284.8	568	86	129	1.0106	1.095
13	Makhtesh Qatan	11	45	-1.8	0.5	-7.9	2.4	<b>288.0</b>	10	99	41	1.0103	1.091
14	Mitzpe Ramon	9	38	-2.7	1.0	-13.6	4.2	284.1	865	96	69	1.0106	1.096

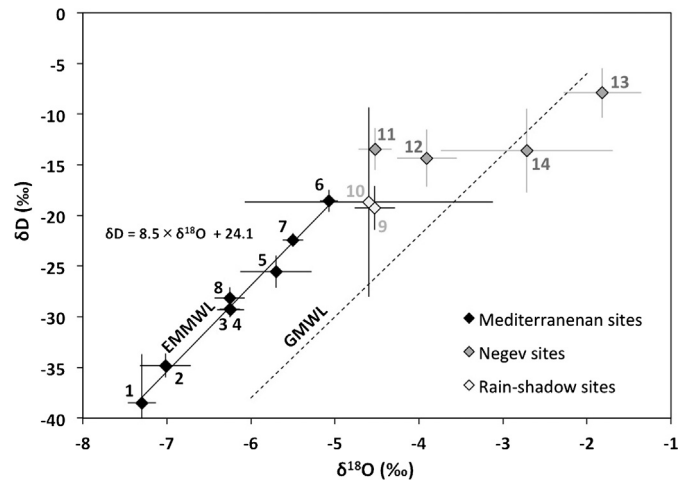


**Fig. 2.**  $\delta^{18}\text{O}_p$  vs.  $\delta D_p$  weighted mean and yearly weighted mean standard error for all sites. The Mediterranean sites fall along the EMMWL (solid black line). The GMWL is presented as reference. The site numbers correspond to Table 1.

than hydrogen. The offset from equilibrium conditions is defined as d-excess and is calculated as  $d = \delta D - 8 \times \delta^{18}\text{O}$ . Precipitation in many parts of the world exhibit a  $d = 10$  and thus fall on the Global Meteoric Water Line (GMWL) defined as  $\delta D = 8 \times \delta^{18}\text{O} + 10$  (Craig, 1961).

## 2. Methods

Isotopic compositions of rainwater from 13 sites in Israel were collected and analyzed by A. Ayalon and M. Bar-Matthews from the Geological Survey of Israel (Ayalon et al., 2004). An additional site (Bet Dagan) with a very long precipitation record was added to the data set from the WISER database ([http://www-naweb.iaea.org/napc/ih/IHS\\_resources\\_isohis.html](http://www-naweb.iaea.org/napc/ih/IHS_resources_isohis.html), accessed 25/8/15). These 14 sites span almost the entire length of Israel; they have a precipitation range of 40 to 1400 mm/yr (Fig. 1) and an elevation range 0 to 1600 m above sea level. The resolution and collection time vary between sites. The longest and most detailed record (daily resolution) is from the Soreq Cave, spanning 1995–2013. The rest of the sites have sparser data, both in the number of years the data were collected and their resolution, which varies between daily and monthly (Table 1).

To assess the long-term value of  $\delta_p$ , we first calculated annually weighted means using:

$$\delta_p = \frac{\sum(\delta_{\text{event}} \times \text{rainfall}_{\text{event}})}{\sum \text{rainfall}} \quad (5)$$

The long term weighted mean was calculated using the annually weighted means and a weighted mean standard error was calculated for each site (Eq. (4.22) in Bevington and Robinson, 2003). The  $\delta^{18}\text{O}_p$  was plotted vs.  $\delta D_p$  from each site and a least square trend-line was fit to the data (Fig. 2). To evaluate the empirical correlations of  $\delta_p$  with rainfall amount, distance from the ocean (continentality) and altitude effects (Gat, 1996),  $\delta^{18}\text{O}_p$  and  $\delta D_p$  were plotted vs. average rainfall amounts, elevation and distance from the sea of each site (calculated as the distance to the nearest coast) (Fig. 3).

## 3. Results

The differences in the thermodynamic and kinetic properties of hydrogen and oxygen result in different magnitudes of response to hydrological processes. Thus plotting both isotopic systems can illuminate these processes. The compiled data from all sites (Fig. 2

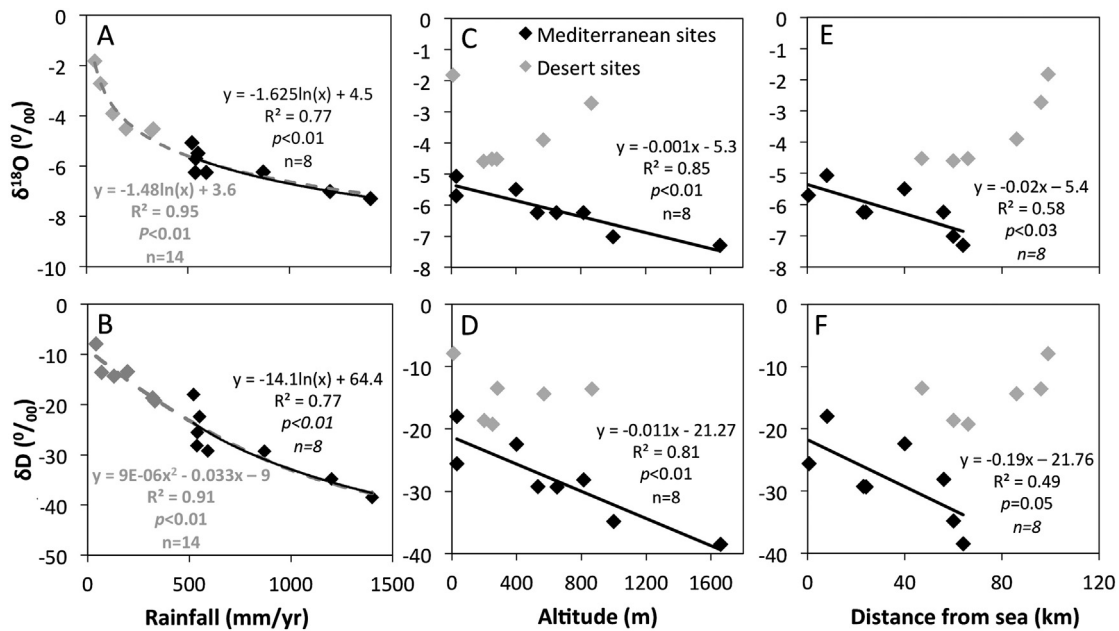


**Fig. 3.** a and b.  $\delta^{18}O_p$  and  $\delta D_p$  vs. annual rainfall amounts. Regression lines were fit to all sites (dashed gray line) and separately for the Mediterranean sites (solid black). c and d.  $\delta^{18}O_p$  and  $\delta D_p$  vs. altitude. e and f.  $\delta^{18}O_p$  and  $\delta D_p$  vs. distance from the Mediterranean coast. Regression lines were fit to the Mediterranean sites (solid black). The desert sites do not fall on the Mediterranean trend line due to the affect of evaporation during precipitation.

and Table 1) show that plotting  $\delta^{18}O_p$  vs.  $\delta D_p$  enables distinguishing between three groups of sites. The first group is composed of sites located in the Mediterranean climate region (henceforth, Mediterranean sites). These sites fall on a straight line (solid line in Fig. 2 and solid black line in Fig. 5) with a least-square fit of:

$$\delta D_p = 8.5 \times \delta^{18}O_p + 24.1 \quad (R^2 = 0.99) \quad (6)$$

A linear fit assumes variance only in the Y-axis ( $\delta D$ ), therefore we also calculated an orthogonal fit that takes into account variations in both axes. The orthogonal fit is:  $\delta D_p = 8.6 \times \delta^{18}O_p + 24.7$ , which is not significantly different from the least square fit. The slope of the best-fit line differs from the East Mediterranean Meteoric Water Line (EMMWL) defined by Gat and Dansgaard (1972) as:  $\delta D_p = 8 \times \delta^{18}O_p + 23$ . The theoretically predicted slope is a function of sea surface temperature (SST), which for a 16.9 °C winter Mediterranean SST (Gat et al., 2003) should be 8.8. Therefore, the best fit-line calculated in Eq. (6) better fits the theoretical value and thus should be used when calculating the deviation from equilibrium values in the Eastern Mediterranean.

In accordance with Dansgaard (1964) and Gat et al. (1996) the rainfall that reaches the Mediterranean sites (those that fall on the EMMWL) is not affected by evaporation during the rainfall events, and therefore, the d-excess of these sites is set by evaporation conditions at the moisture source (i.e. East Mediterranean surface water).

The two other groups of sites fall to the right of the EMMWL. These sites are located in the rain-shadow desert (The Dead Sea Valley) and the Negev Desert in the south of Israel. The reason for this displacement is that rainfall falling over the desert sites most likely undergoes evaporation during the rainfall event (Stewart, 1975; Ayalon et al., 2004). The isotopic compositions from the eastern sites in the Negev (i.e. Mitzpe Ramon and Makhtesh Qatan) fall very close to the GMWL. This is due to a coincidental cancelation of the kinetic fractionation over the Mediterranean during the initial evaporation and the kinetic fractionation during precipitation in the Negev (Figs. 2 and 5).

An additional way to investigate the processes involved in producing the isotopic composition of precipitation is to evaluate

whether these are correlated with climatic and geographic parameters. The most informative of these globally empirical correlations are rainfall amount, elevation and distance from the sea. A strong correlation exists between the annual rainfall amounts and  $\delta^{18}O_p$  ( $R^2 = 0.95$  for an exponential fit) and  $\delta D$  ( $R^2 = 0.91$  for a 2nd order polynomial fit) (dashed lines in Fig. 3a, b). As the dataset is composed of two groups of sites, those that exhibit kinetic fractionation during precipitation and those that do not, individual exponential trend-lines were plotted for the Mediterranean sites (solid black line in Fig. 3a, b).

The Mediterranean sites show a strong correlation between  $\delta^{18}O$  and  $\delta D$  vs. elevation ( $R^2 = 0.85$  and  $0.81$ , respectively) with a magnitude of  $1.3\text{‰}/\text{km}$  and  $10\text{‰}/\text{km}$  for  $\delta^{18}O$  and  $\delta D$ , respectively (Fig. 3c, d). In addition, there is a significant correlation between  $\delta^{18}O$  and  $\delta D$  vs. the distance from the Mediterranean Sea ( $R^2 = 0.58$  and  $0.49$ , respectively) with a magnitude of  $0.2\text{‰}/10 \text{ km}$  and  $2\text{‰}/10 \text{ km}$  for  $\delta^{18}O$  and  $\delta D$ , respectively (Fig. 3e, f). In the desert sites, the kinetic processes overprint the altitude and distance from the sea effects.

#### 4. Discussion

$\delta_p$  from Israel shows good empirical correlations with rainfall amount, altitude and distance from the sea. These processes are all qualitatively correlated. As an air-mass moves eastward, the distance from the sea increases and topography progressively becomes higher, producing colder temperatures and orographic rain. These empirical correlations, though strong, are merely a manifestation of the underlying rainout-distillation process that governs  $\delta_p$ . The distillation process is hard to measure empirically and requires additional information in order to evaluate its properties. In the first part of the discussion, we evaluate whether Rayleigh distillation affects  $\delta_p$  in Israel, by: a) calculating the fraction of remaining vapor for each site and b) constructing a model based on the sea-surface to land temperature gradient. In the second part of the discussion, we use the understanding of the modern principles controlling  $\delta_p$  to constrain the likely hydrological changes that occurred during the LGM in the Mediterranean.

#### 4.1. The effect of Rayleigh distillation on precipitation

The isotopic composition of precipitation ( $\delta_{P(f)}$ ) forms by the condensation of vapor into droplets following the equation:

$$\delta_{P(f)} = \alpha_{l-v(T)} \times (\delta_{v(f)} + 1) - 1 \quad (7)$$

where  $\delta_{P(f)}$  and  $\delta_{v(f)}$  are the isotopic composition of rain and vapor as a function of  $f$  – the fraction of vapor remaining in the cloud (Gat, 1996).

To assess the vapor composition in a cloud as a function of the distillation process ( $\delta_{v(f)}$ ) the Rayleigh distillation model as applied for isotopes, states that (derived from: Gat, 1996):

$$\delta_{v(f)} = (\delta_{v(f=1)} + 1) \times f^{(\alpha-1)} - 1 \quad (8)$$

where  $\delta_{v(f=1)}$  is the initial composition of vapor at the time it is formed (elaborated in 4.1.1). Therefore,  $\delta_P$  as a function of distillation can be calculated by solving for  $\delta_{v(f)}$  using Eqs. (7) and (8):

$$\delta_P = \alpha(\delta_{v(f=1)} + 1)f^{(\alpha-1)} - 1 \quad (9)$$

and the fraction of remaining vapor ( $f$ ) is calculated by rearranging Eq. (9):

$$f = \left[ \frac{\delta_P + 1}{\alpha(\delta_{v(f=1)} + 1)} \right]^{\frac{1}{\alpha-1}} \quad (10)$$

##### 4.1.1. The effect of evaporation on the isotopic composition of vapor

The isotopic composition of the initial vapor ( $\delta_{v(f=1)}$ ) forms during evaporation from the sea surface. The Craig-Gordon model (Craig and Gordon, 1965) divides this process into two steps; in the first step, sea surface water evaporates into a saturated boundary layer and thus follows equilibrium processes;

$$\delta_{V(eq)} = \frac{(\delta_{sw} + 1)}{\alpha_{v-l(T)}} - 1 \quad (11)$$

where  $\delta_{sw}$  is the isotopic composition of seawater and the equilibrium fractionation factor is a function of the SST (Eqs. (3) and (4)). The second step involves diffusion through an unsaturated layer which results in kinetic fractionation ( $\Delta\epsilon_{sw-v(NH)}$ ), which is a function of normalized humidity (NH – the atmospheric vapor content normalized to saturated vapor at SST). Lower NH will result in higher  $\Delta\epsilon_{sw-v(NH)}$ . Therefore the initial vapor that forms above the sea ( $\delta_{V(f=1)}$ ) is:

$$\delta_{V(f=1)} = \frac{(\delta_{sw} + 1)}{\alpha_{v-l(T)}} - 1 - \Delta\epsilon_{sw-v(NH)} \quad (12)$$

By rearranging Eq. (12) it is possible to solve for  $\Delta\epsilon_{sw-v(NH)}$ :

$$\Delta\epsilon_{sw-v(NH)} = \frac{(\delta_{sw} + 1)}{\alpha_{v-l(T)}} - 1 - \delta_{V(f=1)} \quad (13)$$

Thus, to calculate  $f$  for each site using Eq. (10), the following parameters are required: a) the average isotopic composition of Mediterranean Sea water ( $\delta_{sw}$ ); b) the equilibrium fractionation factor ( $\alpha_{l-v(T)}$ ) for the evaporation process (requires: average SST); c) the kinetic fractionation factor ( $\Delta\epsilon_{sw-v(NH)}$ ) (requires: average NH over the Mediterranean and the relation between the magnitude of kinetic fractionation and NH); d) the initial isotopic composition of the vapor ( $\delta_{V(f=1)}$ ) and e) ground temperature at each rainfall monitoring station which will be used to calculate the equilibrium fractionation factor ( $\alpha_{l-v(T)}$ ) of the rainfall condensation. In the following paragraphs these parameters will be derived and the contribution of the distillation effect on  $\delta_P$  in Israel will be evaluated.

##### 4.1.2. Stable Isotopes in Mediterranean Sea water and vapor

Gat et al. (2003) analyzed Mediterranean water, vapor, SST, NH and storm track directions during the winter of 1995. In this paper, the authors claim that the isotopic composition of the Mediterranean vapor falls along the EMMWL, albeit with a large scatter (Fig. 6 in Gat et al., 2003). Here we suggest a new interpretation of the raw data collected by Gat et al. (2003) that accounts quite well for the NH, SST and isotopic composition of the Mediterranean water vapor and enables us to quantify  $\Delta\epsilon_{sw-v(NH)}$ .

When plotting the data Gat et al. (2003) collected from the deck of the ship, it is evident that there are two distinct groups that follow two trend lines (Fig. 4). Group A consists of samples 9, 11–18, 20–22, 24–25 and follows an orthogonal linear fit of:

$$\delta D = 2.74 \times \delta^{18}O - 48.8 \quad (14)$$

Group B consists of samples 1–8, 10, 13–14, 19 and follows an orthogonal linear fit of:

$$\delta D = 4.9 \times \delta^{18}O - 25.55 \quad (15)$$

Sample 23 is an outlier that does not fit into either of the groups.

Based on the synoptic maps and the ship's logbook, Gat et al. (2003) noted rainy conditions during the collection of 9 samples (Nos. 1, 2, 3, 5, 6, 7, 8, 10, 19). All of these samples are part of group B and none of group A. Only 3 samples from group B (4, 13, 14) were not associated with rainfall events. Though, as rainfall was not directly observed during the sampling but deduced later on, we chose to interpret group B as a whole as collected during rainfall events. The reason for the difference in the slopes of the trend lines of both groups is not clear. A possible explanation could be that during rainout the vapor content becomes more depleted (Gat, 1996) shifting the vapor measurements to more negative values. For this reason, henceforth, only group A will be assumed to represent the vapor over the Mediterranean.

To assess the effect of NH on  $\delta_v$ , we calculated the isotopic composition of vapor at equilibrium with the Mediterranean sea-surface ( $\delta_{v(eq)}$ ) using Eq. (11). For the calculation we used an isotopic composition of Mediterranean seawater ( $\delta_{sw}$ ) of:  $\delta^{18}O = 1.25\text{‰}$  (average of data from: Gat et al., 2003) and  $\delta D = 8\text{‰}$  (Gat et al., 1996). The average SST used is:  $16.9^\circ\text{C}$  (Gat et al., 2003). The result of Mediterranean  $\delta_{v(eq)}$  is:  $\delta^{18}O_{v(eq)} = -8.73\text{‰}$  and  $\delta D_{v(NH=1)} = -74.23\text{‰}$ . The  $\delta_{v(eq)}$  falls very close to the trend line predicted by group A, enabling us to use  $\delta_{v(eq)}$  as a reference point to measure the magnitude of the kinetic fractionation. In this way, the distance of each measured vapor point from  $\delta_{v(eq)}$  is the kinetic fractionation factor (as can be seen graphically in Fig. 4a). The calculated kinetic fractionation factor at each site can then be plotted vs.  $1 - \text{NH}$  (Fig. 4b, c), the resulting trend-lines are:

$$\Delta\epsilon^{18}O_{(NH)} = -8.74 \times (1 - \text{NH}) \quad (r^2 = 0.90) \quad (16)$$

$$\Delta\epsilon D_{(NH)} = -20.82 \times (1 - \text{NH}) \quad (r^2 = 0.92) \quad (17)$$

The consistency of the measured  $\delta_{v(NH)}$  (Group A) with the calculated  $\delta_{v(eq)}$  (based on SST) enable an adequate quantification of  $\Delta\epsilon^{18}O_{(NH)}$  and  $\Delta\epsilon D_{(NH)}$  for the Mediterranean. The standard error of the estimate is  $0.5\text{‰}$  and  $6\text{‰}$  for  $\Delta\epsilon^{18}O_{(NH)}$  and  $\Delta\epsilon D_{(NH)}$ , respectively.

Molecular diffusivity theory predicts that  $\Delta\epsilon_{(NH)} = (1 - h) \times \theta \times n \times C_k$ , where  $C_k$  is a constant describing the ratio of heavy to light isotope molecular diffusivity ( $C_k(^{18}O) = 28.5\text{‰}$  and  $C_k(D) = 25.11\text{‰}$ ),  $\theta$  is the ratio of molecular diffusive transport resistance to the total sum of molecular and turbulent transport and  $n$  is an additional weighing factor that accounts for the magnitude of turbulent wind conditions (assumed to be 0.5 over the ocean) (Gat, 1996). The coefficients of  $(1 - \text{NH})$  in Eqs. (16) and (17) are equal

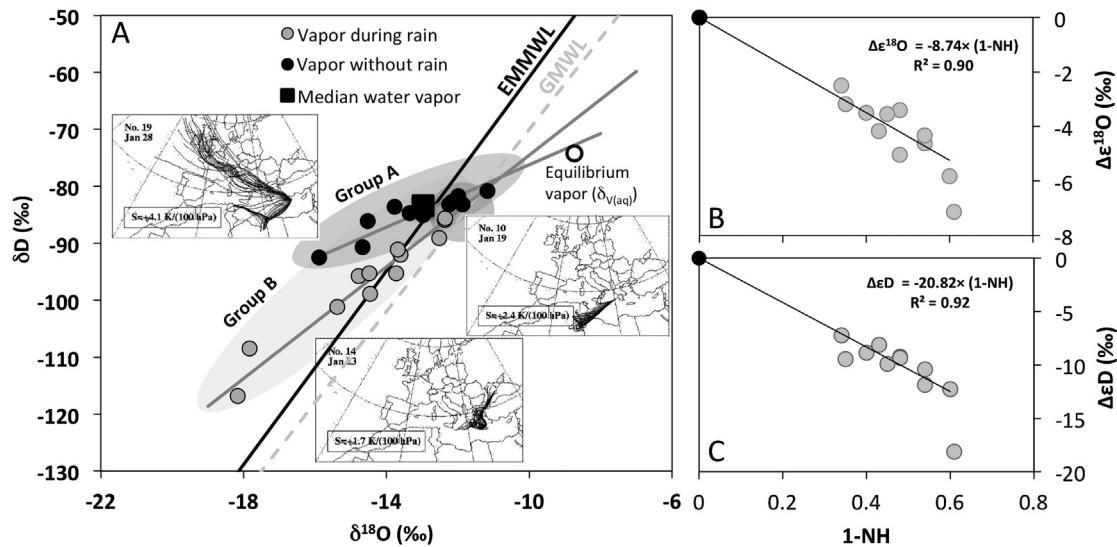


**Fig. 4.** Mediterranean vapor data. **a.**  $\delta^{18}\text{O}$  vs.  $\delta\text{D}$ , where the vapor data is divided into 1) vapor measured during times with no rainfall (black circles and solid black trend-line and 2) vapor measured during active rainfall (gray circles and solid gray trend-line). Error bars ( $1\text{‰}$  and  $0.1\text{‰}$  for  $\delta\text{D}$  and  $\delta^{18}\text{O}$ , respectively) are smaller than the symbols and are thus not plotted. Shaded ellipses represent three groups of vapor data based on the meteorological systems that prevailed during the time they were sampled. The three synoptic maps (Gat et al., 2003) are typical examples of the meteorological systems that correspond to each shaded ellipse is adjacent to it. **b.** The magnitude of the kinetic fractionation of  $\delta^{18}\text{O}_V$  ( $\Delta\epsilon^{18}\text{O}_{(\text{NH})}$ ) as a function of normalized humidity; the gray points are the distance of each vapor measurement from the zero kinetic fractionation (black circle,  $\text{NH} = 1$ ,  $\Delta\epsilon_{\text{sw-v}} = 0$ ) along the x-axis in Fig. 4a, the lower most point was omitted when calculating the trend-line. **c.** Same as plot 4b for  $\Delta\epsilon\text{D}_{(\text{NH})}$  (along the y-axis in Fig. 4a).

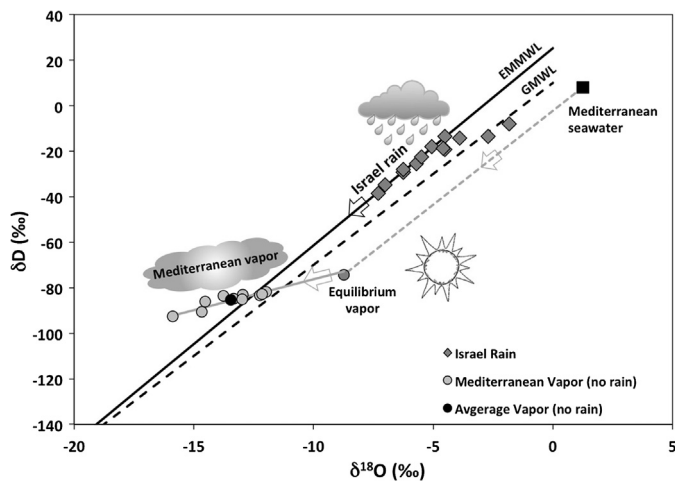


**Fig. 5.**  $\delta^{18}\text{O}$  vs.  $\delta\text{D}$  for the full isotopic hydrological cycle of Mediterranean seawater and vapor and Israel precipitation. The figure is based on the actual data (points and trend-lines). In addition, the schematic processes that govern the cycle (evaporation by heat/sun light, cloud formation and precipitation) are presented.

to  $\theta \times n \times C_k$ , which result in  $\theta(^{18}\text{O}) = 0.6$  and  $\theta(\text{D}) = 1.2$  for vapor over the Mediterranean. The result for  $\theta(^{18}\text{O})$  is in agreement with predicted values for the Mediterranean ( $\sim 0.5$ , Gat, 1996). The result for  $\theta(\text{D})$  is not possible as  $0 < \theta < 1$ . A possible explanation for this discrepancy is that  $\delta\text{D}$  is more sensitive than  $\delta^{18}\text{O}$  to small changes in ocean temperature. The equilibrium values of  $\delta^{18}\text{O}_V$  were calculated using  $\delta^{18}\text{O}_{\text{sw}}$  measurements conducted by Gat et al. (2003) simultaneously with the vapor measurements.  $\delta\text{D}_{\text{sw}}$  were not measured by Gat et al. (2003), requiring us to use  $\delta\text{D}_{\text{sw}}$  data from a previous cruise ( $\delta\text{D}_{\text{sw}}$  is  $\sim 8\text{‰}$ , Gat et al., 1996). This could produce the observed deviation of the calculated  $\theta(\text{D})$  from the theoretical one. Coupled  $\delta\text{D}_{\text{sw}}$  and  $\delta\text{D}_V$  are required to assess this possible source of error in  $\Delta\epsilon\text{D}_{(\text{NH})}$ .

The variability of  $\text{NH}$  over the Mediterranean and the associated composition of the vapor are most likely the outcome of different synoptic patterns. These can be addressed using the synoptic maps given in Gat et al. (2003). From these data it seems that there are

three distinct meteorological conditions that have different isotopic values and hence, different  $\text{NH}$  (Fig. 4a). The first, are systems that originate in the Atlantic Ocean and traverse Europe, they have enriched isotopic values ( $\delta^{18}\text{O} = -11$  to  $-14\text{‰}$ ,  $\delta\text{D} = -80$  to  $-85\text{‰}$ ) and respectively high  $\text{NH}$  (0.75–0.45). The second are systems that are more local and seem to reside over Eastern Europe and have more depleted isotopic values ( $\delta^{18}\text{O} = -14$  to  $-16\text{‰}$ ,  $\delta\text{D} = -90$  to  $-110\text{‰}$ ) and respectively low  $\text{NH}$  (0.45–0.25). The third are systems that take a southern path, these are not represented well in the dataset collected by Gat et al. (2003), and therefore, it is hard to draw conclusions about them. Typical examples of the three meteorological conditions are presented in Fig. 4a. The reason why these three groups have very different isotopic values is unclear at this point and is most likely due to different air mass histories and different mixing proportions of Atlantic and Mediterranean vapor. It is also interesting to note, that the intercept between group A and B falls directly on the GMWL (Fig. 4a). This might indicate that Mediterranean evaporation is not the sole moisture source and that N. Atlantic moisture with a d-excess of  $\sim 10\text{‰}$  reaches the E. Mediterranean (i.e. the E. Mediterranean system might be more complicated than a simple “closure assumption”, Good et al., 2015). Nonetheless, the differences in the isotopic composition of these systems strengthens a point made by Gat and Carmi (1987), that any interpretation of variations in the isotopic composition of rainfall in the Levant must take into account possible changes in the isotopic compositions of these systems and their frequency.

For the purpose of assessing the magnitude of the distillation process, the long-term isotopic composition of the vapor ( $\delta_V(f=1)$ ) and the respective  $\text{NH}$  are required. This can be calculated in two ways: a) the median of the vapor measurements over the source, which based on Gat et al. (2003) is  $\delta^{18}\text{O} = -12.97\text{‰}$  and  $\delta\text{D} = -83.4\text{‰}$  and b) graphically, this value is the intercept of the EMMWL ( $\delta\text{D} = 8.5 \times \delta^{18}\text{O} - 24.1$ ) with the trend-line describing the vapor of Group A ( $\delta\text{D} = 2.74 \times \delta^{18}\text{O} - 48.8$ ) (Figs. 4a and 5), which gives a value of  $\delta^{18}\text{O} = -12.7\text{‰}$  and  $\delta\text{D} = -83.5\text{‰}$ . These two ways of calculating  $\delta_V(f=1)$  were derived by very different ways; the first is a simple average of the vapor measurements over the ocean, whereas the second is derived from the trend-line of long-term rainfall measurements. Their similarity strength-

**Table 2**  
Measured (columns 1 and 2) and modeled (columns 3–6) Rayleigh distillation parameters of the Mediterranean sites.

Site	$f$ (from measured $\delta^{18}\text{O}$ )	$f$ (from measured $\delta\text{D}$ )	$e_{(s)}$ (model)	$f$ (model)	$\delta^{18}\text{O}$ (model)	Residual ( $\delta^{18}\text{O}_{\text{model}} - \delta^{18}\text{O}_{\text{measured}}$ )
Hermon	0.60	0.61	8.2	0.43	-11.05	-3.75
Neve Ativ	0.63	0.65	10.6	0.55	-8.35	-1.33
Peqin	0.68	0.69	12.3	0.64	-6.92	-0.68
Mikhmanim	0.68	0.70	12.8	0.67	-6.47	-0.22
Haifa Port	0.74	0.75	16.7	0.87	-4.01	1.69
Bet Dagan	0.78	0.81	15.7	0.82	-4.54	0.53
Soreq	0.74	0.76	14.2	0.74	-5.51	-0.02
Jerusalem	0.68	0.71	12.9	0.67	-6.40	-0.15

ens the reliability of both data sets. Using the latter of these measurements the long-term average kinetic fractionation can be calculated (Eq. (13)) as:  $\Delta\epsilon^{18}\text{O}_{(\text{NH})} = -12.7 + 8.7 = -4\text{‰}$  and  $\Delta\epsilon\text{D}_{(\text{NH})} = -83.5 + 74.2 = -9.3\text{‰}$ . Using equation (16) and the calculated  $\Delta\epsilon^{18}\text{O}_{(\text{NH})}$  the average NH over the Mediterranean is 54%. Using equations 17 and the calculated  $\Delta\epsilon\text{D}_{(\text{NH})}$  the average winter NH over the Mediterranean is 55%.

#### 4.1.3. Surface temperature at the rainfall collection sites

To calculate the fractionation factor between vapor and liquid ( $\alpha_{l-v}(T)$ , Eqs. (3) and (4)) which is a function of temperature, we used average ground temperatures for the rainy months (Dec, Jan and Feb) from 44 stations in Israel spanning 1995–2012, (measured by the Israel Meteorological Service – <http://www.ims.gov.il/IMS/CLIMATE/ClimaticAtlas/TempNormals.htm>, accessed 19/8/15). Some stations are located in close proximity to the precipitation monitoring stations, for these stations, the average temperature at the station was used directly (regular font in Table 1). To assign a temperature to the monitoring stations that do not have temperature stations in their close proximity we calculated a multiple linear regression of the average DJF temperature of all 44 stations as a function of elevation and latitude:

$$T = 17.92 - 0.00554 \times M - 0.0056 \times L/1000 \quad (R^2 = 0.8) \quad (18)$$

where  $T$  is the temperature in Celsius,  $M$  is elevation in meters and  $L$  is latitude in Israeli Transverse Mercator (ITM). From this least square fit we derive a model temperature for each of the remaining stations (bold font in Table 1). A standard error of the mean of  $0.3\text{ °C}$  ( $1\sigma$ ) was calculated by comparing the model data to the measured data.

#### 4.1.4. Calculating the fraction of remaining vapor for each site

In the previous sections, the necessary parameters for calculating the distillation effect on  $\delta_p$  in Israel were derived. Using Eq. (10), we calculated the fraction of remaining vapor in the cloud above each rainfall measuring station in Israel. We use the initial composition of vapor at the time it formed (calculated in the previous section as  $\delta^{18}\text{O} = -12.7\text{‰}$  and  $\delta\text{D} = -83.5\text{‰}$ ), the ground temperature (derived for the measured and modeled values) and the measured  $\delta_p$  of each rainfall measuring station.

The Rayleigh models for both  $\delta^{18}\text{O}$  and  $\delta\text{D}$  are in agreement and set the fraction of remaining vapor in the cloud during its pass over Israel at 75%–60% (Table 2). This fraction decreases linearly as a function of distance from the Mediterranean Sea (Fig. 6a). Based on this data, the cloud rains out  $\sim 25\%$  over the Mediterranean, and an additional 20% during its passage over Israel.

The distillation calculation is based on ground temperatures at each rainfall station and the average SST measured by Gat et al. (2003). Though, the actual temperatures that control the isotopic composition are the condensation temperatures at the base of the cloud. Thus, a correction is required to account for the initial vapor temperature and the temperature of the clouds during the rainout

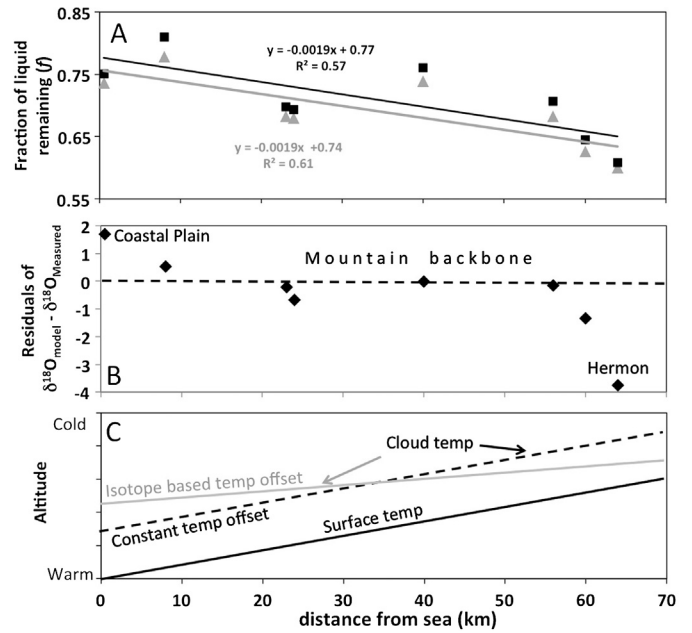


**Fig. 6.** a. The fraction of liquid remaining in the cloud ( $f$ ) for each of the Mediterranean sites plotted vs. the distance from the Mediterranean.  $f$  was calculated using a Rayleigh distillation model for  $\delta^{18}\text{O}$  (black square) and  $\delta\text{D}$  (gray triangle). b. Residuals of the Rayleigh distillation model of the isotopic composition of rainfall in Israel minus the measured weighted mean of the isotopic composition of rainfall from the Mediterranean sites in Israel. The residuals are plotted vs. the distance from the Mediterranean Sea. There are three distinct regions: the mountainous region which Rayleigh distillation model predicts the isotopic composition to a high degree and the coastal plain and Mt. Hermon that the model deviates from measured values. c. A schematic diagram showing the temperature/altitude as a function of the distance from the Mediterranean coast, explaining why the model does not predict well the isotopic composition of rain in the coastal plain and Mt. Hermon. The model uses ground and sea-surface temperatures (solid black line) and assumes a constant temperature offset between the ground and the base of the cloud (dashed black line) where the fractionation occurs. The results of the model do not agree with a constant temperature offset, rather they require a lower temperature gradient (solid gray line), such a gradient would explain why the measured isotopic composition in the coastal plain is more depleted than the model predicts and why the measured isotopic composition in Mt. Hermon is more enriched than the model predicts.

process. Assuming that a typical Levantine rain cloud has an elevation of 500–1000 m above ground and applying a dry adiabatic lapse rate would set the cloud base temperature at 5–10 $^{\circ}\text{C}$  colder than that at the surface. We repeated the distillation calculations to account for the ground to base of the cloud temperature offset. The results show that the fraction of remaining vapor in the cloud decreases by  $\sim 5\%$ , which is not significantly different from those derived from the ground temperature values (75–60%).

#### 4.1.5. Modeling the isotopic composition of the rainfall

In the previous sections, we showed that  $\delta_p$  in Israel correlates well with the amount, altitude and continental effects that are all empirically based correlations. To assess the driver of these empiric-

ical relations, a model of  $\delta^{18}\text{O}_p$  at each rainfall station was constructed by combining the Rayleigh distillation equation (Eq. (9)) with the Clausius–Clapeyron relation (after: Criss, 1999: 112). The fraction of remaining vapor in the cloud ( $f$ ) is calculated using the sea-surface ( $T_{sw}$ ) to land temperature ( $T_{\text{rainfall}}$ ) gradient of each site:

$$f = e_s(T_{\text{rainfall}})/e_s(T_{sw}), \quad (19)$$

where  $e_s$  is the saturated vapor pressure calculated using the August–Roche–Magnus approximation of the Clausius–Clapeyron relation that states the relation of saturated vapor pressure ( $e_s$ ) with temperature ( $T$  in °C) (Bürger et al., 2014):

$$e_s(T) = 6.1094e^{[17.625T/(T-243.04)]} \quad (20)$$

The model precipitation  $\delta^{18}\text{O}_{\text{model}}$  are then compared to the measured  $\delta^{18}\text{O}_{\text{measured}}$  and the residuals are plotted vs. the distance from the Mediterranean coast (Fig. 6b and Table 2). The results divide the Mediterranean sites into 3 regions: a) sites located in the mountainous region of Israel (including Soreq Cave) where the model predicts the average  $\delta^{18}\text{O}_p$  to within 0.6‰ of the observed values, b) coastal plain sites which are more depleted than what would be expected based only on ground temperature and c) Mt. Hermon in the northern tip of Israel that shows values that are enriched in respect to that expected based solely on ground temperature. The remarkable similarity of the model and measured data in the mountainous region indicates that a Rayleigh distillation process driven by the sea surface to land temperature gradient is a major control on  $\delta_p$  in Israel. The empirical correlation with distillation, amount, altitude and continental effects shown above, are thus fundamentally a by-product of the sea surface to land temperature gradient.

A possible explanation for the differences between measured and model data of the coastal plain and in Mt. Hermon would be that the temperatures used in this model are ground temperatures and not the cloud temperatures (as explained above). The model assumes that the sea surface to land temperature gradient remains constant throughout the whole rainout process. This assumption seems to work for the mountainous region but not for the coastal plain sites or the Mt. Hermon site. A possible resolution would be if the surface to cloud offset were larger over the coast and would decrease as the cloud moves inland (Fig. 6c). A 2‰ enrichment, as seen in the coastal plain sites, can be explained by a 2.5°C larger ground to cloud temperature offset (i.e. the temperature at the base of the cloud is 2.5°C colder than predicted by the ground temperature). The same reasoning can be applied for Mt. Hermon where a 3.5‰ depletion can be explained by 5°C smaller ground to cloud offset.

#### 4.2. Constraints on $\delta_p$ during the Last Glacial Maximum

Based on the understating of the importance of the distillation process on modern precipitation, we constructed a model that describes the full hydrological cycle of sea surface water, evaporation, distillation and precipitation during the LGM (25–20 ka). The composition of the LGM East Mediterranean sea-surface water was calculated using the  $\delta^{18}\text{O}$  recorded in planktonic foraminifera (*G. ruber* =  $3.2\text{‰} \pm 0.1\text{‰}$  VPDB) (Almogi-Labin et al., 2009), corrected for a sea surface temperature of  $10\text{°C} \pm 0.5$  during the winter months (7°C colder than present, Almogi-Labin et al., 2009), and converted to the VSMOW scale (Eq. (4) in Arbuszewski et al., 2010 modified from Bemis et al., 1998) resulting in  $\delta^{18}\text{O}_{sw} = 2.11\text{‰}$  VSMOW. Using Eq. (11) the  $\delta^{18}\text{O}$  of vapor at equilibrium with the sea surface would have been  $-8.5\text{‰}$ . The average  $\delta^{18}\text{O}_c$  in the Soreq Cave during the LGM was  $-3.1\text{‰} \pm 0.1$  VPDB (data from: Bar-Matthews et al., 2003). This value was temperature corrected

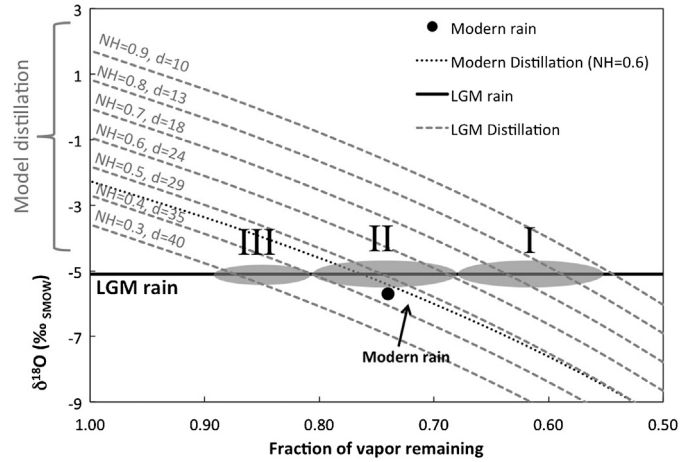


Fig. 7. The  $\delta^{18}\text{O}_p$  over Soreq Cave as a function of distillation intensity. The modern distillation process and  $\delta^{18}\text{O}_p$  over Soreq Cave are presented in black (dotted and circle, respectively). The gray dashed lines represent modeled distillation paths governed by different normalized humidity (NH) values over the Mediterranean (0.3–0.9). The d-excess ( $d = \delta D_{v(f=1)} - 8.7 \times \delta^{18}\text{O}_{v(f=1)}$ ) associated with these NH values was calculated using the temperature corrected  $\delta^{18}\text{O}_{sw}$  (2.11‰) and the corresponding  $\delta D_{sw}$  (18.5‰) calculated using an equilibrium slope in  $\delta^{18}\text{O}$  vs.  $\delta D$  space (9 at  $10\text{°C}$ ). The composition of LGM  $\delta^{18}\text{O}_p$  over Soreq is presented as a solid black line. The gray ovals represent three possible scenarios that can explain the  $\delta^{18}\text{O}_p$  over Soreq during the LGM (see text for elaborate discussion of these scenarios).

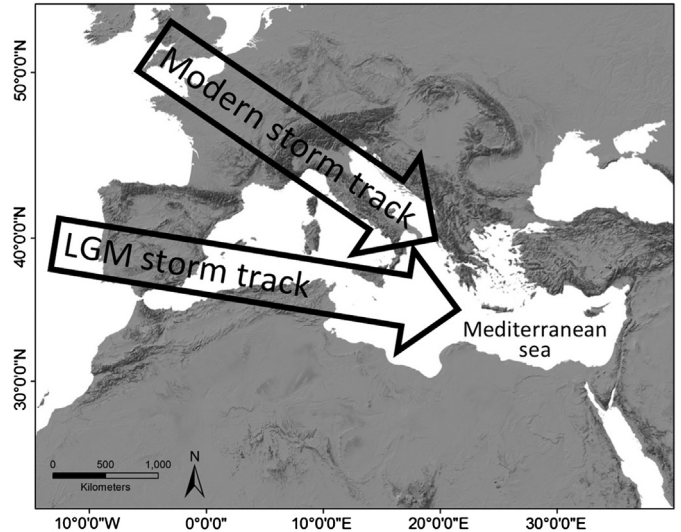


Fig. 8. Modern and proposed LGM storm tracks over the Mediterranean.

(Kim and O’Neil, 1997) using a 5°C winter temperature (assuming a 7°C decrease in temperature relative to present, identical to the East Mediterranean) and converted to the VSMOW scale, resulting in  $\delta^{18}\text{O}_p = -5.1\text{‰}$  VSMOW.

To quantify the full system, two additional parameters are needed: NH above the Mediterranean and the amount of distillation that occurred before reaching Soreq Cave (from Eq. (10)). Based on the modern relation of  $\Delta\epsilon_{sw-v(NH)}$  (Eq. (16)) and a suite of NH values (0.3–0.9) a model was constructed that shows possible distillation paths that could produce the Soreq LGM value of  $\delta^{18}\text{O}_p = -5.1\text{‰}$  (Fig. 7). To calculate the d-excess, we first calculated the theoretical slope of the meteoric water line for a  $10\text{°C}$  LGM Mediterranean sea and used the offset of the modern measured minus theoretical slope ( $8.8 - 8.5 = 0.3$ ) to get the slope of the LGM meteoric water line ( $9 - 0.3 = 8.7$ ). Then using Eqs. (16) and (17) we calculated the d-excess (Fig. 7).

To assess the error on  $f$  from all parameters excluding NH, we performed an error propagation analysis using a Monte Carlo sim-



ulation (see Appendix A). The results of the error analysis show that for each ascribed NH value (each realization), the propagated error of  $f$  is 3% ( $1\sigma$ ) (Fig. S1). Thus the uncertainty in the estimate of  $f$  is largely associated with the uncertainty in the estimation of NH over the Mediterranean, whereas the uncertainty of the other parameters only minimally contributes to the overall uncertainty (Fig. S2).

The results of the model (Fig. 7) show that there are three types of scenarios that could produce the LGM rainfall composition: I) during the LGM, the amount of distillation over Israel was 10–20% larger and NH over the Mediterranean was 10–20% higher than present; II) the amount of distillation over Israel was the same as today and the normalized humidity was 10% lower over the Mediterranean, and III) during the LGM, the amount of distillation was smaller and the NH was 20% lower than today.

To assess which one of these three end member scenarios is the most plausible, additional paleoclimate proxies are evaluated. Fluid inclusions in Soreq speleothems (Matthews et al., 2000; McGarry et al., 2004) show a d-excess of 10–20‰ during the LGM (i.e. 10‰ lower than present), these values fit scenario I and to a lesser extent scenario II, but rule out scenario III. Clumped isotopes in Soreq speleothems (Affek et al., 2014) show a 10 °C cooling during the LGM. Assuming a 7 °C cooling in the Mediterranean (Almogi-Labin et al., 2009) results in an increased Mediterranean Sea – Soreq temperature gradient. Using the reasoning for the modern climatic conditions presented above, an increase in the Mediterranean Sea – Soreq temperature gradient would result in an increase in the magnitude of distillation, which would fit scenario I. Though, the uncertainty in temperature reconstructions (SST and Soreq clumped isotope temperature), complications due to soil evaporation (e.g. Bar-Matthews et al., 1996) and the greater distance from the sea due to lower sea level during the LGM does not completely rule out scenario II. The high-stand of Lake Lisan during the LGM (+200 m of mean Holocene values) and the  $\text{HCO}_3^-$  budget of the lake require an increase in precipitation over Israel (Enzel et al., 2008). Both scenario I and II could fit this record: scenario I requires an increase in the amount of precipitation of each rainfall event (i.e. increased distillation), and scenario II requires an increase in the number of rainfall events without an increase in the amount of precipitation of each event (i.e. without a change in the magnitude of distillation). These three independent paleoclimate proxies point to scenarios I and II as the most plausible, though, due to measurement precision and natural scattering, the ability to differentiate which one of the two scenarios is most plausible is not possible at this point.

Scenario I requires that during the LGM the Mediterranean had NH values of 70–90%, 10–30% higher than present, closer to the global average (~80%–90%, Meriviat and Jouzel, 1979). The modern low humidity over the Mediterranean forms when dry air from Europe encounters the warm Mediterranean Sea (Ziv et al., 2006). During the LGM, a moisture path over Europe could not have resulted in higher NH values due to the extensive ice cover over Europe that would have resulted in higher-pressure systems driving drier air into the Mediterranean. Therefore, a possible solution would be that the Atlantic vapor shifted southward over passing the warmer Southern Europe (Fig. 8) (for similar results see: Florineth and Schlüchter, 2000, and Enzel et al., 2008 for a more detailed synoptic overview and discussion of this shift). A southern shift of this route would result in air masses with higher humidity entering the Mediterranean and produce precipitation over Israel with a smaller d-excess.

## 5. Conclusions

Long-term averages of the isotopic composition of precipitation from 14 sites in Israel and vapor data from the Mediter-

anean allow the full hydrological cycle of sea surface water, vapor, distillation, precipitation and evaporation to be assessed. The results show that the long-term isotopic composition of precipitation in Israel is governed primarily by the composition of the Mediterranean, normalized humidity over the Mediterranean and the sea-surface to land temperature gradient that drives the distillation effect. The isotopic composition of precipitation is empirically correlated with the amount of precipitation ( $r^2 = 0.95$ ), altitude ( $r^2 = 0.85$ ) and distance from the ocean ( $r^2 = 0.58$ ). These high correlations are driven by the distillation process via a temperature decrease as a function of altitude and distance from the coast. The isotopic composition of precipitation in sites located in the desert region is affected by evaporation during precipitation process, which does not affect sites located in the Mediterranean region.  $\delta^{18}\text{O}$  values from Soreq Cave speleothems and from East Mediterranean *G. ruber* were used to construct a model of the isotopic composition of precipitation for the LGM (25–20 ka). The model was constrained using data from speleothem fluid inclusions and clumped isotope and data regarding Lake Lisan hydrology during the LGM. The results suggest two possible reconstructions of the LGM hydrology: I) during the LGM, the amount of distillation over Israel and NH over the Mediterranean were higher than present; II) the amount of distillation over Israel and NH over the Mediterranean were roughly the same as today. Scenario I requires a significant increase in the NH over the Mediterranean, such an increase was most plausibly the result of a southern shift of the moisture sources over southern Europe bringing in warm-moist Atlantic vapor directly into the Mediterranean resulting in higher normalized humidity values and a smaller d-excess in rain over Israel.

## Acknowledgements

We thank Yochanan Kushnir, Boaz Luz, Yehouda Enzel, Ian Clark, Yael Kiro, Mordechai Stein and Yehoshua Kolodny for helpful and most appreciated advice and the Lamont–Doherty Earth Observatory Organic Geochemistry group whose weekly discussions facilitated much of the ideas in this paper. Lamont–Doherty Earth Observatory contribution number 8066.

## Appendix A. Error propagation of LGM reconstruction

Bellow we derive the equations used and perform a Monte Carlo error propagation of the fraction of remaining vapor.

Combining Eqs. (10) and (12)

$$f = \left[ \frac{(\delta_p + 1000)}{\alpha_{sq} \left( \frac{(\delta_{sw} + 1000)}{\alpha_{sst}} - \Delta\epsilon \right)} \right]^{\frac{1}{\alpha_{sq} - 1}}$$

Accounting for kinetic fractionation from Eq. (16).

$$f = \left[ \frac{(\delta_p + 1000)}{\alpha_{sq} \left( \frac{(\delta_{sw} + 1000)}{\alpha_{sst}} + 8.74(1 - \text{NH}) \right)} \right]^{\frac{1}{\alpha_{sq} - 1}}$$

Converting  $\delta_p$  to  $\delta_{\text{CaCO}_3}$  and converting from VPDB to VSMOW using (Kim and O'Neil, 1997).

$$f = \left[ \frac{\frac{(1.03086 \times \delta_{\text{CaCO}_3} + 30.86) + 1000}{\alpha_{\text{CaCO}_3}}}{\alpha_{sq} \left( \frac{(\delta_{sw} + 1000)}{\alpha_{sst}} + 8.74(1 - \text{NH}) \right)} \right]^{\frac{1}{\alpha_{sq} - 1}}$$

Converting  $\delta_{\text{foram}}$  from VPDB to VSMOW using  $\delta^{18}\text{O}_{\text{foram(VSMOW)}} = \delta^{18}\text{O}_{\text{foram(PDB)}} + ((T - 16.5)/4.8) + 0.27$  from: Bemis et al. (1998).

$$f = \left[ \frac{\frac{(1.03086 \times \delta_{\text{CaCO}_3} + 30.86) + 1000}{\alpha_{\text{CaCO}_3}}}{\alpha_{sq} \left( \frac{(\delta_{\text{foram}} + \frac{T_{sst} - 16.5}{4.8} + 0.27) + 1000}{\alpha_{sst}} + 8.74(1 - \text{NH}) \right)} \right]^{\frac{1}{\alpha_{sq} - 1}}$$

The parameters used including uncertainties

$$\delta_{\text{CaCO}_3(\text{VPDB})} = -3.1\text{‰} \pm 0.1 \quad (\text{Bar-Matthews et al., 2003}).$$

$$\delta_{\text{foram}(\text{VPDB})} = 3.2\text{‰} \pm 0.1 \quad (\text{Bar-Matthews et al., 2003}).$$

The uncertainty of  $\delta^{18}\text{O}_{\text{foram}}$  is not presented in Almogi-Labin et al., 2009, as they used the same instrument (VG SIRA II mass spectrometer) as Bar-Matthews et al. (2003), we took the instrumental uncertainty from the later.

$$\delta^{18}\text{O}_{\text{sw}} = \delta^{18}\text{O}_{\text{foram}(\text{VPDB})} + ((T - 16.5)/4.8) + 0.27 \pm 0.7\text{‰}$$

from: Bemis et al. (1998).

$$T_{\text{sst}} = 10\text{‰C} \pm 1 \quad (\text{Almogi-Labin et al., 2009}).$$

$$T_{\text{cave}} = 5 + 273.15 = 278.15\text{‰K} (\text{Almogi-Labin et al., 2009}) \pm 0.5.$$

$$\alpha_{\text{sst}} = 1.0107 \pm 0.00011 \quad (\text{Horita and Wesolowski, 1994})$$

using percent of error in  $1000 \ln \alpha$ .

$$\alpha_{\text{sq}} = 1.0112 \pm 0.00011 \quad (\text{Horita and Wesolowski, 1994})$$

using percent of error in  $1000 \ln \alpha$ .

$$\alpha_{\text{CaCO}_3} = 1.0330 \pm 0.000103 \quad (\text{Kim and O'Neil, 1997})$$

using percent of error in  $1000 \ln \alpha$ .

$$\Delta \varepsilon^{18}\text{O}_{(\text{NH})} = \pm 0.5\text{‰}.$$

NH = 0.8 (for demonstrating uncertainty).

Error propagation using Monte Carlo simulation.

Each parameter was ascribed 10,000 normally distributed random values with a mean = 0 and standard deviation = 1. These were multiplied by the uncertainty and added to the parameter value. The fraction of remaining vapor was calculated 10,000 times. The probability density function was plotted (Fig. S1). The results show a normally distributed  $f$  with a range of ~20% and standard deviation of 3%. These results indicate that the uncertainty in the estimate of  $f$  is largely associated with the uncertainty in the estimation of NH over the Mediterranean, whereas the uncertainty of the other parameters only minimally contributes to the overall uncertainty (Fig. S2).

## Appendix B. Supplementary material

Supplementary material related to this article can be found online at <http://dx.doi.org/10.1016/j.epsl.2016.10.017>.

## References

- Affek, H.P., Matthews, A., Ayalon, A., Bar-Matthews, M., Burstyn, Y., Zaarur, S., Zilberman, T., 2014. Accounting for kinetic isotope effects in Soreq 1 Cave (Israel) speleothems. *Geochim. Cosmochim. Acta* 143, 303–318.
- Almogi-Labin, A., Bar-Matthews, M., Shriki, D., Kolosovsky, E., Paterne, M., Schilman, B., Ayalon, A., Aizenshtat, Z., Matthews, A., 2009. Climatic variability during the last ~90 ka of the southern and northern Levantine basin as evident from marine records and speleothems. *Quat. Sci. Rev.* 28, 2882–2896.
- Angert, A., Lee, J., Yakir, D., 2008. Seasonal variations in the isotopic composition of near-surface water vapour in the eastern Mediterranean. *Tellus B* 60, 674–684.
- Arbuszewski, J., deMenocal, P., Kaplan, E., Farmer, C., 2010. On the fidelity of shell-derived  $\delta^{18}\text{O}_{\text{seawater}}$  estimates. *Earth Planet. Sci. Lett.* 300, 185–196.
- Ayalon, A., Bar-Matthews, M., Sass, E., 1998. Rainfall-recharge relationships within a karstic terrain in the Eastern Mediterranean semi-arid region, Israel:  $\delta^{18}\text{O}$  and  $\delta\text{D}$  characteristics. *J. Hydrol.* 207, 18–31.
- Ayalon, A., Bar-Matthews, M., Schilman, B., 2004. Rainfall Isotope Characteristics at Various Sites in Israel and the Relationships with Unsaturated Zone Water. Israel Geological Survey report GSI/16/04. 15 pp.
- Ayalon, A., Bar-Matthews, M., Frumkin, A., Matthews, A., 2013. Last glacial warm events on Mount Hermon; the southern extension of the Alpine karst range of the east Mediterranean. *Quat. Sci. Rev.* 59, 43–56.
- Bar-Matthews, M., Ayalon, A., Matthews, A., Sass, E., Halicz, L., 1996. Carbon and oxygen isotope study of the active water-carbonate system in a karstic Mediterranean cave: implications for paleoclimate research in semi-arid regions. *Geochim. Cosmochim. Acta* 60, 337–347.
- Bar-Matthews, M., Ayalon, A., Kaufman, A., 1997. Late Quaternary paleoclimate in the eastern Mediterranean region from stable isotope analysis of speleothems at Soreq Cave, Israel. *Quat. Res.* 47, 155–168.
- Bar-Matthews, M., Ayalon, A., Kaufman, A., Wasserburg, G.J., 1999. The Eastern Mediterranean paleoclimate as a reflection of regional events: Soreq Cave, Israel. *Earth Planet. Sci. Lett.* 166, 85–95.
- Bar-Matthews, M., Ayalon, A., Gilmour, M., Matthews, M., Hawkesworth, C., 2003. Sea-land isotopic relationships from planktonic foraminifera and speleothems in the Eastern Mediterranean region and their implications for paleorainfall during interglacial intervals. *Geochim. Cosmochim. Acta* 67, 3181–3199.
- Bemis, E.B., Spero, H.J., Bihma, J., Lea, D.W., 1998. Reevaluation of the oxygen isotopic composition of planktonic foraminifera: experimental results and revised paleotemperature equations. *Paleoceanography* 13 (2), 150–160.
- Bevington, P., Robinson, D.K., 2003. *Data Reduction and Error Analysis for the Physical Sciences*, 3rd ed. McGraw-Hill, New York, NY.
- Bürger, G., Heistermann, M., Bronstert, A., 2014. Towards subdaily rainfall disaggregation via Clausius-Clapeyron. *J. Hydrometeorol.* 15, 1303–1311.
- Craig, H., 1961. Isotopic variations in meteoric waters. *Science* 133 (3465), 1702–1703.
- Craig, H., Gordon, L.I., 1965. Deuterium and oxygen 18 variations in the ocean and the marine atmosphere. In: Tongiorgi, E. (Ed.), *Stable Isotopes in Oceanographic Studies and Paleotemperature*. Laboratorio Di Geologia Nucleare, Pisa, pp. 9–130.
- Criss, R.E., 1999. *Principles of Stable Isotope Distribution*. Oxford University Press, New York. 254 pp.
- Dansgaard, W., 1964. Stable isotopes in precipitation. *Tellus* 16 (4), 436–468.
- Enzel, Y., Amit, R., Dayan, U., Cruvi, O., Kahana, R., Ziv, B., Sharon, D., 2008. The climatic and physiographic controls of the eastern Mediterranean over the late Pleistocene climates in the southern Levant and its neighboring deserts. *Glob. Planet. Change* 60, 165–192.
- Florineth, D., Schlüchter, C., 2000. Alpine evidence for atmospheric circulation patterns in Europe during the Last Glacial Maximum. *Quat. Res.* 54, 295–308.
- Frumkin, A., Ford, D.C., Schwarcz, H.P., 1999. Continental oxygen isotopic record of the last 170,000 years in Jerusalem. *Quat. Res.* 51, 317–327.
- Gat, J.R., 1996. Oxygen and hydrogen isotopes in the hydrologic cycle. *Annu. Rev. Earth Planet. Sci.* 24 (1), 225–262.
- Gat, J.R., Carmi, I., 1970. Evolution of the isotopic composition of atmospheric water in the Mediterranean Sea area. *J. Geophys. Res.* 75 (15), 3039–3048.
- Gat, J.R., Carmi, I., 1987. Effect of climate changes on the precipitation patterns and isotopic composition of water in a climate transition zone: case of the Eastern Mediterranean Sea area. In: *The Influence of Climate Change and Climatic Variability on the Hydrologic Regime and Water Resources*, Proceedings of the Vancouver Symposium. August 1987. In: IAHS Publ., vol. 168, pp. 513–523.
- Gat, J.R., Dansgaard, W., 1972. Stable isotope survey of the fresh water occurrences in Israel and the Northern Jordan Rift Valley. *J. Hydrol.* 16, 177–212.
- Gat, J.R., Shemesh, A., Tziperman, E., Hecht, A., Georgopoulos, D., Bastruk, O., 1996. The stable isotope composition of water of the eastern Mediterranean Sea. *J. Geophys. Res.* 101, 6441–6451.
- Gat, J.R., Klein, B., Kushnir, Y., Roether, H., Wernli, H., Yam, R., Shemesh, A., 2003. Isotope composition of air over the Mediterranean Sea: index of the air-sea interaction pattern. *Tellus B* 55, 953–965.
- Good, S.P., Noone, D., Kurita, N., Benetti, M., Bowen, G.J., 2015. D/H isotope ratios in the global hydrologic cycle. *Geophys. Res. Lett.* 42, 5042–5050.
- Horita, J., Wesolowski, D.J., 1994. Liquid-vapor fractionation of oxygen and hydrogen isotopes of water from the freezing to the critical temperature. *Geochim. Cosmochim. Acta* 58, 3425–3437.
- Kim, S-T., O'Neil, J.R., 1997. Equilibrium and nonequilibrium oxygen isotope effects in synthetic carbonates. *Geochim. Cosmochim. Acta* 61 (16), 3461–3475.
- Kolodny, Y., Stein, M., Machlus, M., 2005. Sea-rain-lake relation in the Last Glacial East Mediterranean revealed by  $\delta^{18}\text{O} - \delta^{13}\text{C}$  in Lake Lisan aragonites. *Geochim. Cosmochim. Acta* 69, 4045–4060.
- Majoube, M., 1971. Fractionnement en oxygène-18 et en deutérium entre l'eau et sa vapeur. *J. Chem. Phys.* 55, 1423–1436.
- Matthews, A., Ayalon, A., Bar-Matthews, M., 2000. D/H ratios of fluid inclusions of Soreq Cave (Israel) speleothems as a guide to the Eastern Mediterranean Meteoric Line relationships in the last 120 ky. *Chem. Geol.* 166, 183–191.
- McGarry, S., Bar-Matthews, M., Matthews, A., Vaks, A., Schilman, B., Ayalon, A., 2004. Constraints on hydrological and paleotemperature variations in the Eastern Mediterranean region in the last 140 ka given by the  $\delta\text{D}$  values of speleothem fluid inclusions. *Quat. Sci. Rev.* 23, 919–934.
- Merlivat, L., Jouzel, J., 1979. Global Climatic interpretation of the deuterium - oxygen 18 relationship for precipitation. *J. Geophys. Res.* 84, 5029–5033.
- Orland, I.J., Burstyn, Y., Bar-Matthews, M., Kozdon, R., Ayalon, A., Matthews, A., Valley, J.W., 2014. Seasonal climate signals (1998–2008) in a modern Soreq Cave stalagmite as revealed by high-resolution geochemical analysis. *Chem. Geol.* 363, 322–333.

- Pausata, F.S.R., Battisti, D.S., Nisancioglu, K.H., Bitz, C.M., 2011. Chinese stalagmite  $\delta^{18}\text{O}$  controlled by changes in the Indian monsoon during a simulated Heinrich event. *Nat. Geosci.* 4, 474–480.
- Stewart, M.K., 1975. Stable isotope fractionation due to evaporation and isotopic exchange of falling waterdrops: application to atmospheric processes and evaporation of lakes. *J. Geophys. Res.* 80 (9), 1133–1146.
- Ziv, B., Dayan, U., Kushnir, Y., Roth, C., Enzel, Y., 2006. Regional and global atmospheric patterns governing rainfall in the Southern Levant. *Int. J. Climate* 6, 55–73.